Earth and Planetary Science Letters 560 (2021) 116810

Contents lists available at ScienceDirect

Earth and Planetary Science Letters

www.elsevier.com/locate/epsl

Deformation-enhanced recrystallization of titanite drives decoupling between U-Pb and trace elements

Stacia M. Gordon [a,*], Christopher L. Kirkland [b,1], Steven M. Reddy [b], Hannah J. Blatchford [c], Donna L. Whitney [c], Christian Teyssier [c], Noreen J. Evans [b], Bradley J. McDonald [b]

[a] Department of Geological Sciences and Engineering, University of Nevada-Reno, NV, USA
[b] School of Earth and Planetary Sciences, John de Laeter Centre, Curtin University, Western Australia, Australia
[c] Department of Earth & Environmental Sciences, University of Minnesota-Twin Cities, MN, USA

ARTICLE INFO

Article history:
Received 6 May 2020
Received in revised form 24 September 2020
Accepted 4 February 2021
Available online xxxx
Editor: A. Yin

Keywords:
titanite
u-pb geochronology
trace elements
deformation
UHP terrane
petrochronology

ABSTRACT

Titanite is a common accessory mineral that is useful in determining both age (U-Pb isotopes) and pressure-temperature (P–T) conditions (trace-element composition: Zr, rare earth elements (REE)). However, titanite has a propensity to recrystallize during metamorphism, fluid flow, and deformation, which can result in modifications to its isotopic and trace-element compositions. This modification has implications for the interpretation of titanite dates and the evaluation of pressure–temperature–time paths. The impact of deformation and recrystallization on trace-element mobility in titanite is investigated through microstructural and compositional mapping of titanite crystals from a sheared orthogneiss within an ultrahigh-pressure domain of the Western Gneiss Region (WGR), Norway. Results show that optically coherent titanite single crystals deformed in the dislocation creep regime and recrystallized by the process of grain-boundary migration, forming aggregates of titanite grains. Some of the aggregate grains record Caledonian-exhumation dates, whereas others have an inherited isotopic composition. Individual grains within the aggregate, regardless of their U-Pb isotopic composition, contain patchy zoning that formed during syn- to post-recrystallization fluid alteration and that is characterized by generally decreasing Ca and Ti and increasing Al and Fe from cores to rims. However, Zr and Sr concentrations are broadly zoned with respect to the long axis of the host crystal, without regard for the aggregate grain boundaries. REE do not show any obvious correlation with microstructure or age. These results indicate that many trace elements in titanite are unaffected by multi-stage, deformation-driven recrystallization; in contrast, Pb is variably mobile in these deformed titanite crystals. The combination of microstructural and high-spatial resolution geochemical and isotopic data reveals the potential extent of decoupling between the U-Pb isotopic system and the behavior of trace elements as pressure–temperature conditions change through time.

1. Introduction

The composition and microstructure of some metamorphic minerals can be used to determine the pressure (depth), temperature, and deformation conditions of the deep continental crust and thereby constrain tectonic processes, such as exhumation (e.g. Rubatto, 2002; Engi, 2017). Titanite ($CaTiSiO_5$) is useful in this regard because it occurs in a wide variety of rock types (Frost et al., 2000) and may incorporate significant concentrations of trace elements that provide estimates on the timing (U-Pb; e.g. Frost et al., 2000), temperature and pressure (Zr; Hayden et al., 2008; Kapp et al., 2009) and recrystallization or breakdown of different minerals on the pressure–temperature (P–T) path (rare earth elements [REE] and Sr; e.g. Stearns et al., 2015; Kohn, 2017).

A wide range of closure temperatures have been proposed for titanite based on a combination of experimental and field-based studies (500–>840°C; Cherniak, 1993; Mezger et al., 1991; Spencer et al., 2013; Stearns et al., 2015; Hartnady et al., 2019; Holder et al., 2019). This has led to U-Pb titanite dates being used to estimate the timing of high-temperature metamorphism and >840°C magmatic crystallization (Hartnady et al., 2019) to cooling along retrograde metamorphic P–T paths (e.g. Mezger et al., 1991). Moreover, although inherited titanite has been widely document in some terranes (e.g., Spencer et al., 2013), under certain conditions, titanite is highly reactive and recrystallizes readily (e.g.

* Corresponding author.
E-mail address: staciag@unr.edu (S.M. Gordon).
[1] Timescales of Mineral Systems Group.

https://doi.org/10.1016/j.epsl.2021.116810
0012-821X/

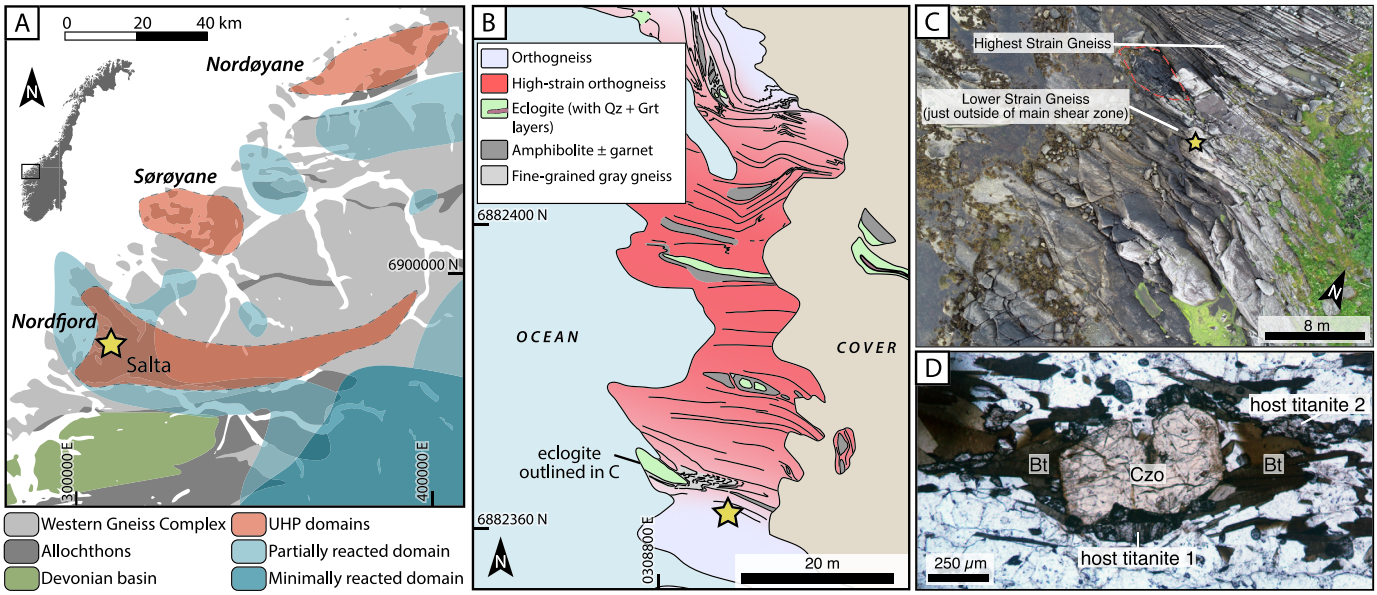

Fig. 1. (a) Simplified geologic map of the Western Gneiss Region, Norway showing the location of the three UHP domains (Nordfjord, Sørøyane, Nordøyane) and the zones of crust that partially to minimally reacted during Scandian tectonics (after Garber et al., 2017). The location of the Salta shear zone is indicated by a star. (b) Simplified map of the Salta shear zone showing the region of high strain intensity and the location (yellow star) of the gneiss sample studied here (after Renedo et al., 2015). The sample was collected from latitude 62.02515 and longitude 5.34541 (using WGS84 datum). (c) Aerial photograph showing the southern portion of the Salta shear zone, with the southernmost eclogite from (b) outlined and the sample location shown again with a star. (d) Photomicrograph of the gneiss showing the location of the two studied host titanite crystals. (For interpretation of the colors in the figure(s), the reader is referred to the web version of this article.)

Kirkland et al., 2016). For example, the breakdown of rutile, ilmenite, and/or zoisite can produce titanite (e.g. Frost et al., 2000), or titanite may recrystallize due to heating, fluids, and/or deformation, as evidenced by a polycrystalline habit, core to rim changes in the isotopic and geochemical composition, and/or the presence of intra-grain dislocations and subgrains (e.g. Lucassen and Becchio, 2003; Müller and Franz, 2004; Storey et al., 2007; Lucassen et al., 2011; Spencer et al., 2013; Bonamici et al., 2015). This reactivity can make the interpretation of titanite U-Pb dates challenging because it may be unclear if the measured dates relate to cooling through the Pb closure temperature or to other processes. For example, during exhumation of high-pressure rocks, new titanite may grow during decompression as rutile becomes unstable (e.g. Spencer et al., 2013; Marsh and Kelly, 2017) or as a result of recrystallization of relict titanite, which may be induced by fluids and/or deformation (e.g. Lucassen and Becchio, 2003; Garber et al., 2017).

In parts of some ultrahigh-pressure (UHP) terranes, inherited titanite grains are present, suggesting that the U-Pb system in some titanite can remain undisturbed during both subduction to mantle depths and subsequent exhumation to the near surface (e.g., Tucker et al., 1987; Spencer et al., 2013; Garber et al., 2017). Extensive titanite geochronology has been conducted across much of the Western Gneiss Region (WGR), a giant (5000 km^2 of UHP rocks/30000 km^2 of HP rocks) ultrahigh-pressure terrane in western Norway (e.g. Tucker et al., 2004; Kylander-Clark et al., 2008; Krogh et al., 2011; Spencer et al., 2013; Garber et al., 2017). Most titanite yield U-Pb dates <405 Ma, interpreted as recording titanite recrystallization or neoblastic growth during cooling and exhumation of the WGR. However, in the southern WGR (Fig. 1), some titanite grains preserve Precambrian isotopic compositions (see 'partially reacted domain' in Fig. 1; Spencer et al., 2013; Garber et al., 2017). Titanite is not predicted to be stable at pressures greater than ~1.2–1.5 GPa (e.g., Spencer et al., 2013) depending on Al–F–OH substitutions (Kohn, 2017); such pressures were far exceeded throughout the WGR during Caledonian orogenesis (Ravna and Terry, 2004; Hacker, 2006). Relict Precambrian grains of titanite, as well as rare Precambrian monazite, the preservation of symplectite in host orthogneisses, and relict Precambrian granulite-facies structures have all been used to argue that regions of the WGR, particularly in the southern WGR, did not significantly deform during Caledonian subduction and subsequent exhumation (e.g. Krabbendam et al., 2000; Hacker et al., 2015; Garber et al., 2017).

Deformation and associated recovery and recrystallization of minerals play a strong role in controlling the rheology of metamorphic rocks (e.g. Urai et al., 1986). For individual minerals, these processes can also affect their isotopic and chemical composition (e.g. Reddy et al., 2006; Erickson et al., 2015; Piazolo et al., 2016). The observed microstructure within the rock can result from a combination of multiple dynamic and/or static recrystallization mechanisms that aim to reduce the strain energy within the grains (e.g. Halfpenny et al., 2012), and each of these mechanisms has the potential to modify the composition of accessory phases important for deciphering the pressure–temperature–time (P–T–t) history of high-grade terranes. Thus, in high-grade, polydeformed terranes such as in the WGR, it is critical to tie the microstructure to different parts of the P–T–t path to reconstruct the tectonic history. Microstructures can preserve useful information for evaluating this tectonic history; however, careful evaluation of how those microstructures relate to the evolving *P–T–strain* path of the host is needed. Many studies have shown that the grain microstructure of high-temperature terranes results from the destruction of intragrain, highly strained features (i.e. dislocations, subgrains, low-angle boundaries) via growth of new relatively dislocation-free grains (e.g. Vandermeer and Juul Jensen, 1998). In comparison, experimental work in combination with electron-backscatter diffraction (EBSD) studies of natural rocks have also shown that microstructures may be preserved during recrystallization (e.g. Bestmann et al., 2005).

Throughout the WGR, there are numerous km- to m-scale wide shear zones that aided in the exhumation of the WGR from mantle depths to the near surface (e.g. Krabbendam and Dewey, 1998; Milnes and Koyi, 2000; Renedo et al., 2015). Here, we evaluate the microstructure of titanite crystals within a well-characterized shear zone in the southern WGR, the Salta shear zone (Fig. 1)

(Cuthbert et al., 2000; Carswell et al., 2003; DesOrmeau et al., 2015; Renedo et al., 2015). We combine EBSD and compositional analysis of titanite crystals to investigate the relationship between microstructural evolution and trace-element modification of critical elements used to document *P–T–strain* conditions and timing of geologic events (e.g. Pb, Zr, Sr, REE). The individual crystals of titanite track a record of reactions that affected the protolith rocks to the WGR as well as the deformation history of the WGR during its exhumation from mantle depths to the near surface.

2. Western Gneiss Region and Salta Shear Zone

The WGR resulted from the collision of Laurentia with Baltica (e.g. Roberts and Gee, 1985). Parts of Baltica were subducted to mantle depths and underwent eclogite-facies metamorphism from ca. 425–400 Ma during the latest (Scandian) phase of Caledonian orogenesis (e.g. see geochronology summary in DesOrmeau et al., 2015; Hacker et al., 2015). The UHP metamorphism is recorded in three domains that contain coesite-bearing eclogite and/or gneiss (Root et al., 2005) (Fig. 1a). Peak metamorphic conditions increase from the southern to the northern UHP domain, from ~2.8 GPa, 700°C to ~3.2–3.6 GPa, 850°C, respectively (Cuthbert et al., 2000; Ravna and Terry, 2004; Hacker, 2006). These domains are separated by regions that have the same lithologies and protoliths but were metamorphosed at HP (Root et al., 2005).

Large-scale (10s of km wide) shear zones bound the WGR (e.g. Roberts and Gee, 1985; Krabbendam and Dewey, 1998), and numerous small-scale (10s of m) shear zones also occur throughout the WGR, including within the three UHP domains (e.g. Milnes and Koyi, 2000; Renedo et al., 2015). These shear zones were active during exhumation of the WGR to mid-crustal depths by ca. 385 Ma (e.g. Kylander-Clark et al., 2008; Spencer et al., 2013; Garber et al., 2017). This study focuses on strongly deformed orthogneiss from one of these small-scale shear zones—the Salta ductile shear zone (Renedo et al., 2015) in the Nordfjord UHP domain (Fig. 1a). The Salta shear zone exposes variably retrogressed eclogite pods enclosed in quartzofeldspathic gneiss across a 60 m wide zone (Fig. 1b,c). The main body of eclogite is tabular (20 x 3–5 m), strongly deformed, and compositionally layered, consisting of omphacite + garnet-rich layers that locally contain garnet–quartz layers. Relict coesite and polycrystalline quartz are found as inclusions in some garnet from the garnet–quartz layers in eclogite (Cuthbert et al., 2000; Renedo et al., 2015). The garnet–quartz layers are interpreted to have been nearly pure coesite with accessory garnet at UHP (Carswell et al., 2003). Polycrystalline quartz has also been found in the host orthogneiss (Wain, 1997). Eclogite-facies metamorphism occurred from ca. 409–401 Ma based on U-Pb zircon and Sm-Nd garnet dates from the layered eclogite (Carswell et al., 2003; DesOrmeau et al., 2015).

Microstructural data from highly elongate omphacite in the eclogite, and quartz fabrics in garnet–quartz eclogite layers and the host orthogneiss, indicate that the shear zone developed at eclogite-facies conditions and remained active during exhumation to amphibolite-facies conditions (Renedo et al., 2015). Both the layered eclogite and the orthogneiss share the same foliation and lineation orientations and evidence for top-to-the-west sense of shear. This shear zone lies in a region interpreted as partially reacted continental crust (Fig. 1a; after Garber et al., 2017) containing both Scandian titanite and inherited Precambrian isotopic compositions in some titanite domains (Spencer et al., 2013; Garber et al., 2017). Only Precambrian zircons and no Scandian grains have been found in a layer-parallel leucosome from this shear zone and pegmatites from other parts of the Nordfjord UHP domain (Gordon et al., 2013; Kylander-Clark and Hacker, 2014). In addition, relict granulites near the shear zone (Krabbendam et al., 2000; Wain et al., 2001) support the limited reactivity of this portion of the WGR.

Variable titanite U-Pb ages have been reported from the WGR. Tucker et al. (1987, 1990, 2004) analyzed titanite from >55 gneiss and leucosome samples across the WGR with a combination of abraded multi-grain and single-grain TIMS analyses. The combined samples define a discordia array between ca. 1660 to 395 Ma. They report that in multiple samples, two types of titanite are observed: one that is coarser grained, darker in color, and blockier versus small, euhedral, yellow to light brown single grains or overgrowths. The latter are interpreted to be syn-metamorphic, neocrystallized Scandian grains, whereas the darker brown, blockier grains yield discordant results and are interpreted to be Gothian, ca. 1650 Ma grains that experienced variable thermally induced Pb loss.

Kylander-Clark et al. (2008) mainly analyzed titanite-bearing gneiss and leucosome samples from northeast and east of the northern and central UHP domains and in and south of the central UHP domain. The majority of the samples from east of the UHP domains yield discordant titanite results, whereas those from within and south of the central domain show mainly Scandian ages. Their discordant results define two main discordia lines with upper intercepts of ca. 940 and ca. 1635 Ma, and lower-intercept ages of ca. 390 Ma.

Subsequently, Spencer et al. (2013) conducted a campaign-style LA-ICP-MS study of >150 titanite-bearing samples from across and between the UHP domains as well as from the eastern WGR. The majority of the samples each define a single $^{238}U/^{206}Pb$–$^{207}Pb/^{206}Pb$ isochron with a Scandian age. These samples have $^{207}Pb/^{206}Pb$ data-defined intercepts ranging between 0.83–0.99, with most clustering at ~0.91 and one sample yielding a lower value of 0.67. In the gneiss and leucosome samples that yield a mix of Precambrian and Scandian dates, the majority reveal a range of Precambrian to Caledonian dates across individual grains; the data did not fall along obvious regression lines in these samples and thus the $^{207}Pb/^{206}Pb$ intercepts are not defined.

Finally, Garber et al. (2017) expanded on the titanite dataset with a detailed petrochronology study on gneisses and leucosome samples from across the WGR. Like the other studies, they document a combination of Precambrian, mixed Precambrian–Caledonian, and recrystallized and neoblastic Caledonian grains. For the samples that define a discordia line, most of the $^{207}Pb/^{206}Pb$ intercepts are between 0.73–1.0. The Caledonian grains are generally more Al-rich and LREE- and Fe-poor in comparison to Precambrian grains. The Caledonian grains have core-to-rim zoning, with the Fe and Al zoning anticorrelated in recrystallized grains versus similar zoning in neoblastic grains. Based on trace-element zoning and the Caledonian age distribution, Garber et al. (2017) interpret that the recrystallized titanite formed as a result of dissolution-reprecipitation. In addition, the study describes recrystallized titanite that is typically found in less deformed, allanite-bearing rocks, whereas fine-grained, more highly strained gneiss more commonly contain neoblastic Caledonian titanite.

To better understand the effects of deformation on titanite recrystallization and composition, several titanite crystals from gneiss within the Salta shear zone were analyzed. Titanite crystals are abundant in this gneiss, are ~100–750 μm in length, and typically subhedral. In compariston, titanite from the gneiss in the middle of the shear zone, where the most intense deformation is observed, are small (<50 μm), making it difficult to analyze intragrain zones using laser-ablation inductively coupled plasma mass spectrometry (LA-ICP-MS). The titanite grains throughout the Salta shear zone are very low in U (Table A1); thus, a smaller spot size for analysis would yield data with such high uncertainties that it would not be useful for comparing intragrain microstructures with the chemical and isotopic composition of that portion of the grain. Therefore, the studied sample was collected from near the mar-

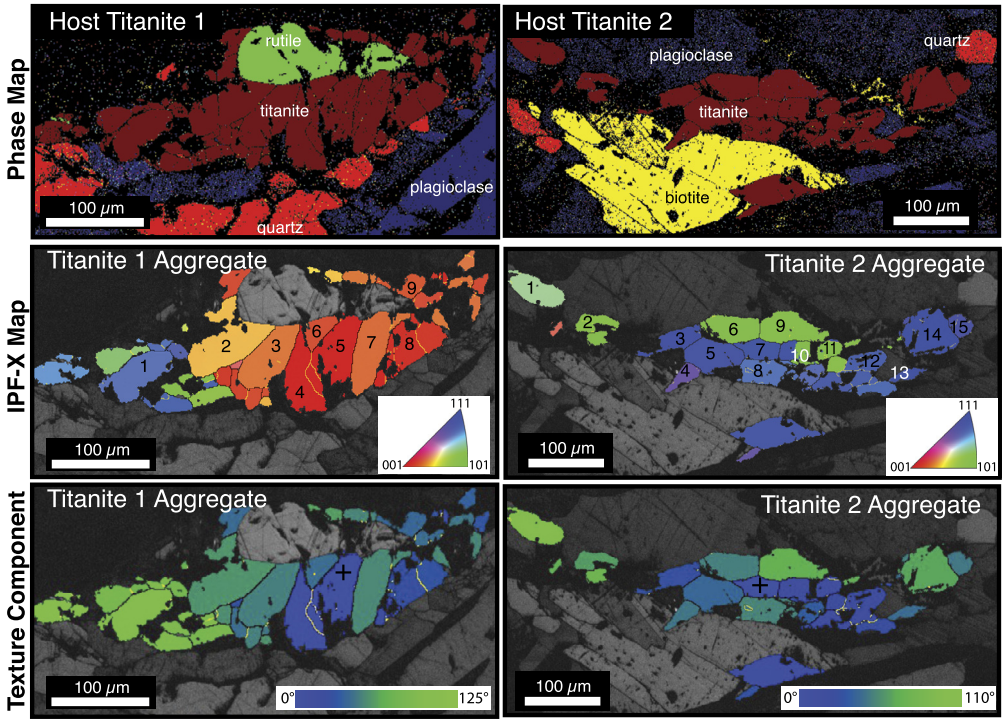

Fig. 2. EBSD phase, inverse pole figure-X, and texture component orientation maps for the two titanite host crystals and grain aggregates studied in detail. The IPF maps are colored relative to a user-defined sample X direction and are overlaid on EBSD band contrast maps. The different aggregate grains are numbered. The texture component maps are also overlaid on EBSD band contrast maps and are made based on the location of the black cross within the interior of the host crystals. For both the IPF-X and the texture component maps, the black lines indicate grain boundaries (>10° misorientation), and the yellow lines, low-angle boundaries (between 2 and 10° misorientation).

gin of the highest strain mylonitic rocks (Fig. 1b,c). The selected gneiss consists of plagioclase + quartz + biotite, with accessory clinozoisite, apatite, zircon, and titanite. The gneiss has undergone significant grain-size reduction due to the shear zone strain and lacks allanite. Thus, the sample falls into a category of gneisses that would more likely contain neoblastic titanite (Garber et al., 2017).

3. Methods

Two clusters of continuous, dark brown titanite within a single thin section were targeted for this study (Fig. 1d). In addition, rutile that is enclosed by one of the titanite clusters was also analyzed. The clusters are similar to titanite described as deformed with numerous subgrains and/or as dynamically recrystallized titanite in Spencer et al. (2013). Within a cluster, the titanite are cracked but lack obvious grain boundaries in an optical image. The crystals were mapped with an electron microprobe (EPMA) and with EBSD to determine chemical and microstructural characteristics. This was followed by LA-ICP-MS analyses to determine the isotopic date and trace-element concentrations (Table A1). The rutile was only analyzed by LA-ICP-MS (Table A2).

3.1. Microstructural analysis

Electron backscatter diffraction maps were collected with an Oxford EBSD detector and Aztec software on a Tescan Mira3 VP field emission scanning electron microscope housed within the Microscopy and Microanalysis Facility in the John de Laeter Centre, Curtin University. A working distance of 20 mm, a 70° stage tilt, a 20 kV accelerating voltage, 4 x 4 binning, and a pixel/step size of 1 μm were used during the analyses. In addition to titanite, neighboring quartz, plagioclase, and biotite were indexed as well as rutile included within one of the titanite clusters. For the entire map area, post processing included correcting for wild spikes and a 5 nearest neighbor zero solutions correction. Further details of the EBSD analyses are included in the supplemental materials. The results are presented in maps and pole figures showing both the orientation relative to inverse pole figure-X (IPF-X) and relative to a specific spot in the grain aggregate (Figs. 2 and 3). For the latter, the spot chosen for the texture component map is located close to the center of the titanite cluster or potential core of the original host crystal. All parts of the two original crystals had recrystallized so we were not able to choose a location that contained the original, non-replaced orientation.

3.2. Compositional analysis

Qualitative X-ray intensity maps were acquired using a JEOL 8530F EPMA at the Centre for Microscopy, Characterisation, and Analysis housed within the University of Western Australia. Analytical conditions were 20 kV accelerating voltage, 100 nA beam current, and a focused beam. A 1 × 1 μm pixel size and 250 ms dwell time per pixel were used to make Al, Ce, Ti, Ca, Fe, Zr, F, and Si X-ray maps. The raw count data were acquired and processed using the Probe Image and CalcImage applications. For all the maps (Fig. 4), the colors are scaled to the raw X-ray counts, with cooler colors representing lower element concentrations, and warmer colors higher concentrations. The color contrast was enhanced to show subtle zoning features using Golden Software's Surfer application.

3.3. Isotopic analysis

The titanites and rutile were analyzed *in situ* using a Resonetics RESOlution M-50A-LR system comprising a Compex 102 193 nm excimer UV laser, connected to an Agilent 7700s quadrupole ICP-MS within the GeoHistory Facility in the John de Laeter Centre at Curtin University. U-Pb isotopes and trace elements were measured during the same ablation. A 33 μm beam was utilized at a

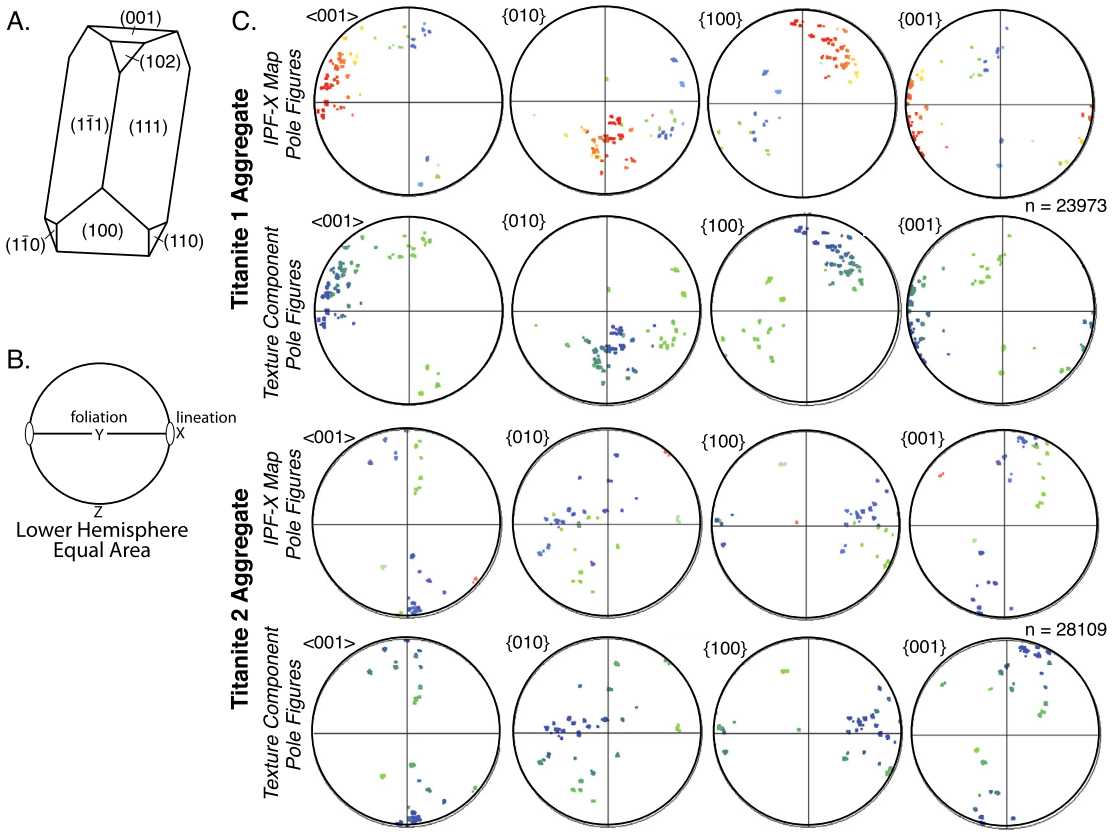

Fig. 3. (a) Orthographic projection of a typical crystal form of titanite (after Paterson and Stephens, 1992); (b) Reference pole figure showing the orientation of the pole figure relative to the sample foliation and lineation; (c) Pole figures of poles to the <001> set of directions and the {010}, {100}, and {001} collection of crystal faces for all parts of the host titanite crystals. The pole figures are colored relative to the IPF-X and texture component maps for each host titanite grain and associated grain aggregates (Fig. 2).

5 Hz laser repetition rate and on-sample laser energy of 2 J/cm^2 was used for the titanite analyses; analyses followed the procedures described in Kirkland et al. (2016). For the rutile analyses, a spot diameter of 22 µm, a repetition rate of 7 Hz, and an on-sample energy of 2.7 J/cm^2 was used for the analyses. For several of the aggregate titanite grains within the overall coherent grain, the analysis consisted of nearly all of the grain, at least in one dimension; therefore, we are not able to assess trace-element zoning in each, individual titanite grain within the grain aggregates. In a few cases, the spot overlapped grain edges (Fig. A1). There are minor inclusions within the titanite grains within host titanite 1, including quartz and K-feldspar. These inclusions are observed in EDS maps and were avoided during the LA-ICP-MS analyses. Both ages and trace element content were determined using Iolite (U_Pb_Geochron4 and Trace Elements data reduction schemes, respectively (Paton et al., 2011)). Further details of the LA-ICP-MS analyses are presented in the supplemental materials.

The isotopic and geochemical composition of titanite may reflect multiple components, including inherited Pb from a precursor phase (e.g., rutile), common Pb, and radiogenic Pb (e.g., Romer and Rötzler, 2003; Lucassen et al., 2010; Stearns et al., 2015; Kirkland et al., 2016; Garber et al., 2017). To account for potential common Pb contributions, titanite dates are first calculated based on a Tera-Wasserburg concordia regression assuming mixing between common and radiogenic Pb on an intergrain level within each cluster of titanite that likely define an original titanite crystal or potentially even a precursor rutile crystal (Fig. 5) (e.g. Stearns et al., 2015). Those analyses included within the mixing line calculation are those that define a clear statistically acceptable regression and share a similar Th/U ratio. Additionally, we calculate intragrain dates to distinguish potentially different grain-scale Pb components (Fig. 6) (e.g. Kirkland et al., 2016). The difference between the U/Pb ratio at the 207-corrected age and the measured isotopic composition is interpreted as an estimate of the amount of common Pb (f207%). To ensure that the results are not biased by the chosen common Pb model, we calculate apparent ages using a variety of different Pb model compositions (with models appropriate for 0 Ma up to 1000 Ma) (Fig. A2). Importantly, the Scandian 207-corrected dates remain dominant no matter what common-Pb composition is used. Hence, neither the form nor the application of the common-Pb model that is used in the correction result in significant differences to the Caledonian-age component; the uncorrected ^{238}U/^{206}Pb dates show the same inherited versus Caledonian age trends as the 207-corrected ages (Table A1).

4. Results

Two titanite crystals near a clinozoisite grain were investigated in detail. The crystals have either a broadly sigmoidal or diamond shape (Fig. 1d). Titanite grain 1 is located directly adjacent to the clinozoisite and is ~250 µm in length. This titanite nearly completely mantles rutile (Fig. 2), a common reaction texture in the host rock and in many high-pressure mafic rocks (e.g., Romer and Rötzler, 2003; Lucassen et al., 2010; Spencer et al., 2013). Titanite grain 2 is located proximal to a pressure shadow associated with the clinozoisite grain and is ~300 µm in length. The EBSD results from the two studied titanite crystals reveal that each apparently-coherent 'grain' is an aggregate of multiple smaller grains, each with straight boundaries, some of which intersect at triple junctions (Fig. 2). In this work, we refer to the coherent titanite crystals 1 and 2 as "host" grains, whereas the smaller crystals that compose the host are referred to as "aggregate" grains.

In host titanite 1, the nine grains making up the aggregate are elongated either perpendicular to the long axis of the relict rutile

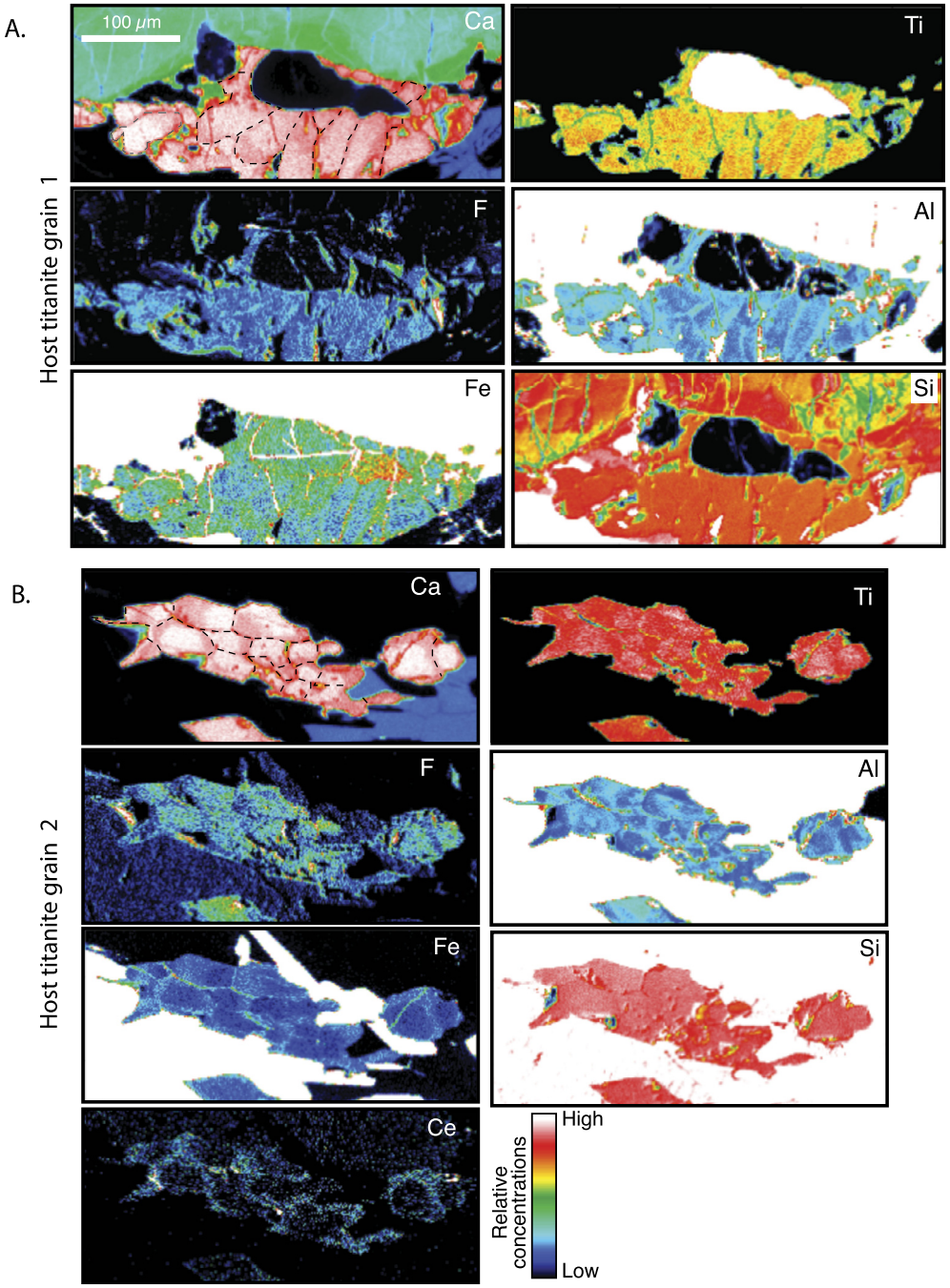

Fig. 4. Electron microprobe X-ray maps of (a) host titanite 1, and (b) host titanite 2. The colors are scaled to the raw X-ray counts, with cooler colors representing lower element concentrations, and warmer colors indicating higher concentrations. The dashed black line in the Ca maps shows the outline of the grains within the aggregate defined by the EBSD data.

grain, or the grains wrap around the rutile that is present in the interior of the titanite aggregate (Fig. 2); the long axis of the rutile is parallel to foliation. Misorientation measurements between adjacent aggregate grains range from 5 to 86°, and there is an overall systematic change in the orientation of grains. The c-axes of the grains are dispersed along a great circle, broadly around the {010} pole (Fig. 3c). In addition, there is a ~90° orientation relationship between the aggregate grains surrounding aggregate grain 1 (near one end of the host titanite grain) and the aggregate grains directly adjacent to the rutile, including grains 2-9, in {100} and {001} orientations (Figs. 2 and 3). The LA-ICP-MS analyses reveal a range of 207-corrected U-Pb dates from 580 to 379 Ma across the aggregate (Figs. 5, 6, and A3). A regression through the analyses yields a lower-intercept age of 402 ± 17 Ma (MSWD = 1.3), with an initial $^{207}Pb/^{206}Pb$ of 0.92 ± 0.30 (2 sigma; data defined y-intercept) (Fig. 5). Aggregate grains 2, 5, and 9 are not included in the regression because of their higher Th/U ratio in comparison to the rest of the aggregate. The aggregate grains with the highest f207% (grains 6 and 9) are both small grains (Table A1) that border the rutile grain; grain 6 is within the interior of the aggregate. Given their small grain size, the spot analysis clipped the grain edges (Fig. A1). The cracks or other spaces along the grain boundaries may have accumulated common Pb resulting in higher f207%. The rutile that is enclosed by host titanite 1 was also analyzed. Two spots on the crystal yield 207-corrected ages of 427 ± 35 Ma and 463 ± 57 Ma (Table A2).

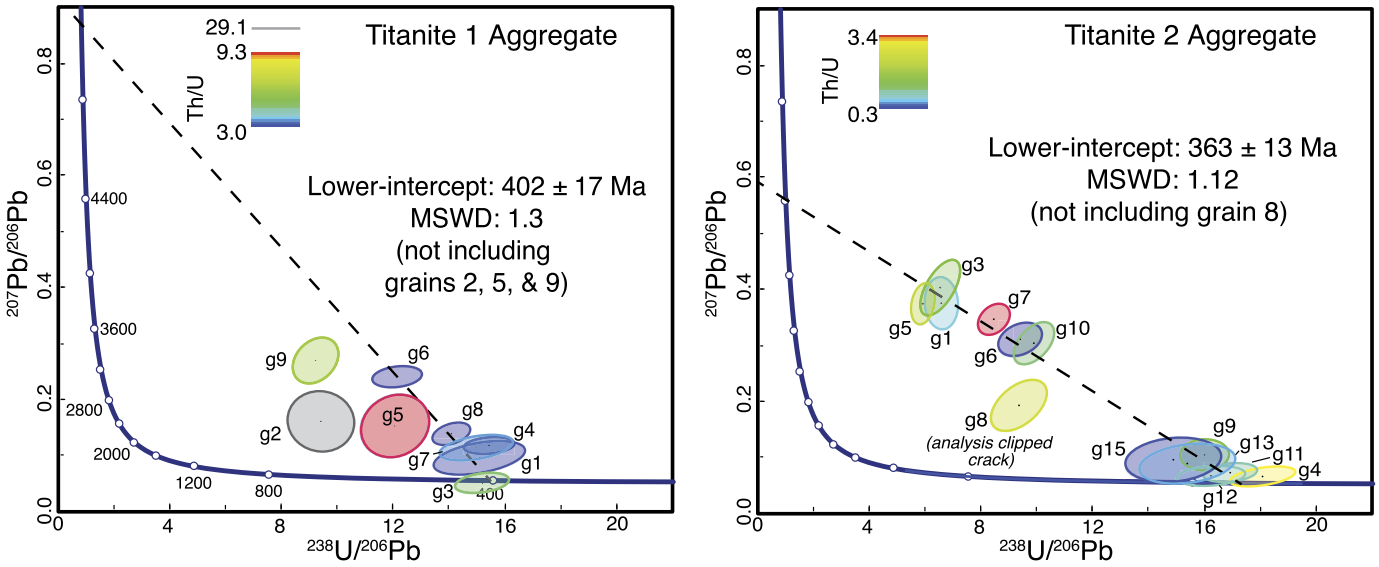

Fig. 5. Inverse concordia diagrams for the analyses across the aggregate of grains associated with host titanite 1 and 2, with the individual spot analyses colored by their Th/U ratio; each ellipse is labeled with the grain number from Fig. 2. For titanite 1, the regression does not include grains 2, 5, or 9 that had higher Th/U values. For titanite 2, the regression does not include grain 8, where the analysis hit a crack.

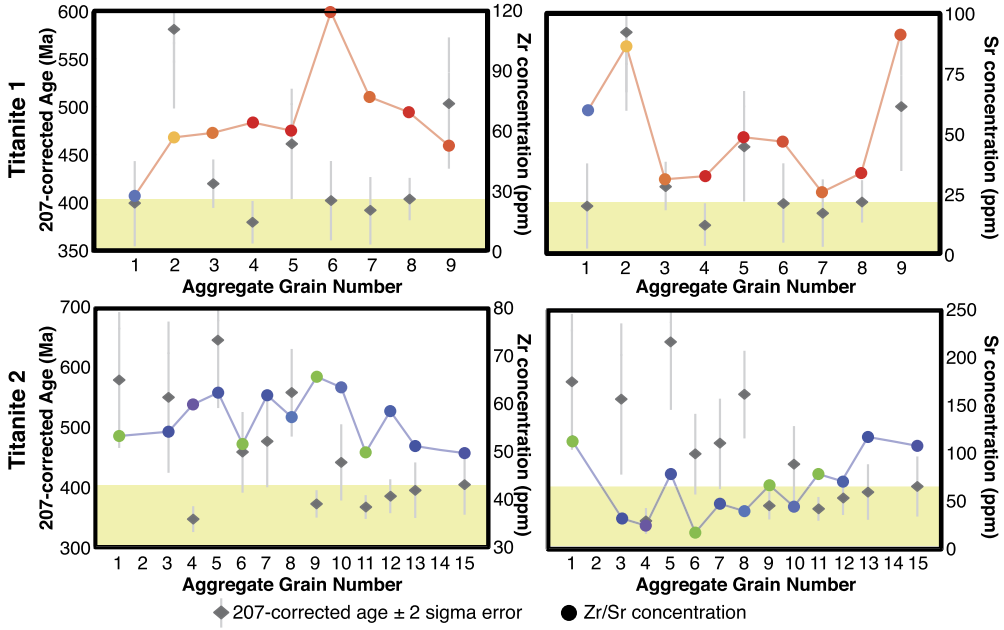

Fig. 6. 207-corrected $^{206}Pb/^{238}U$ ages and Zr and Sr concentrations versus position in the host grain (see Fig. 2) The Zr and Sr symbols are colored relative to the IPF-X map (Fig. 2). The yellow bar represents titanite that recrystallized during Scandian exhumation, based on the U-Pb zircon data of DesOrmeau et al. (2015).

Host titanite grain 2 comprises an aggregate of grains elongated parallel to the main foliation. Misorientation between adjacent aggregate grains range from 21 to 89°. The aggregate grains associated with host titanite grain 2 show more orientation variation than those associated with host grain 1 but also reveal a consistent and systematic variation in crystallographic orientation, in particular in the <001> axes, across the host grain (Fig. 3c). The aggregate grains also yield a spread in 207-corrected dates, ranging from 646 to 347 Ma (Fig. 6). Most of the aggregate grains define a single regression, with a lower-intercept age of 363 ± 13 Ma (MSWD = 1.1; excluding aggregate grain 8 and 14) and an initial $^{207}Pb/^{206}Pb$ of 0.592 ± 0.035 (2 sigma) (Fig. 5). Aggregate grain 8 was ablated partially through a crack, which may have modified the Pb composition (Fig. A1). The analysis through grain 14 ablated through the titanite; therefore, this analysis has very large uncertainties and is not included in any of the regressions and is not shown in figures. Notably, the majority of the grains within the left side of the aggregate all have higher common to radiogenic Pb ratios (i.e., are farther off concordia) in comparison to the majority of the grains that make up the right side of the aggregate (Fig. 5).

X-ray element maps also highlight the multi-grain nature of the titanite aggregate grains (Fig. 4). The individual aggregate grains display distinct patchy zoning for some elements, with broadly decreasing Ca and Ti and increasing Al, Fe, and Ce (only in aggregate grains of host grain 2) concentrations from core to rim. Late fractures cut the individual aggregate grains that make up both host titanite crystals 1 and 2. The fractures are enriched in Fe, Al, and Ca and depleted in Ti, with similar composition to the grain rims.

Trace elements also show variable patterns both within and between the host titanite grains 1 and 2 (Figs. 6, 7, A1). Overall,

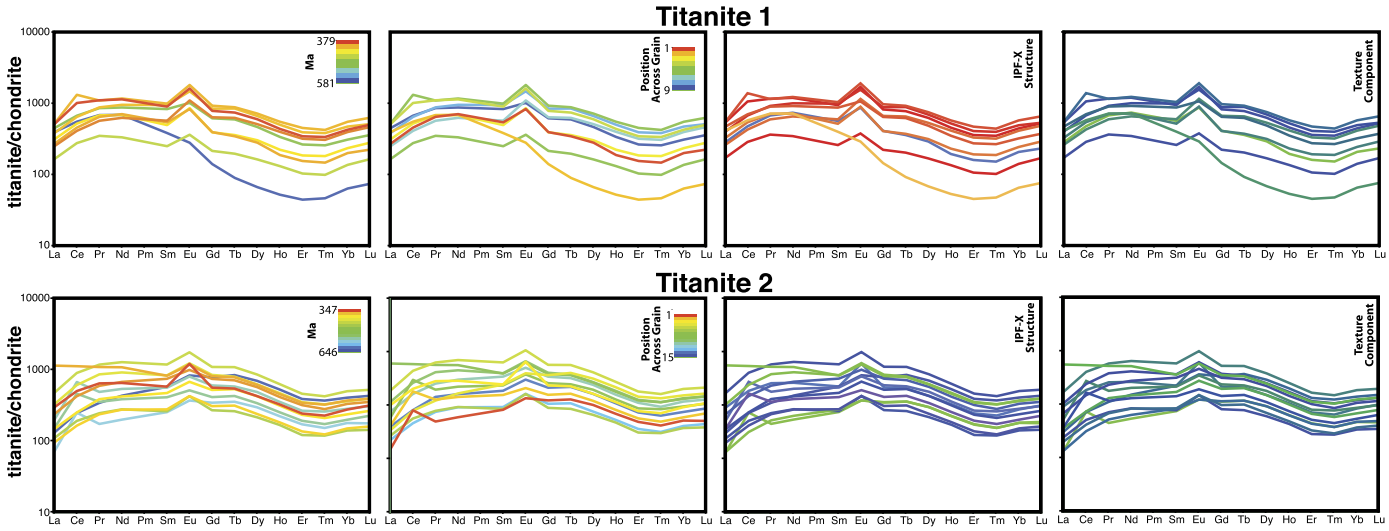

Fig. 7. Rare earth element diagrams for the aggregate of grains associated with host titanite 1 and 2 color coded by the 207-corrected age, by the position across the grain, relative to the IPF-X map and to the texture component map (refer to Fig. 2 for the colors).

the aggregate grains have relatively flat profiles from the LREE to HREE and positive Eu anomalies. There is no correlation among 207-corrected age, position within the aggregate, and REE pattern (Fig. 7). Some of the individual grains within host titanite grains 1 and 2 have higher concentrations of REE, but it does not directly correlate with the degree of misorientation (Fig. 7). Strontium content ranges from 91 to 26 ppm across host titanite grain 1 and from 140 to 22 ppm across host titanite grain 2 (Figs. 6 and A1). In comparison, Zr content ranges from 118 to 29 ppm across host titanite grain 1 and a narrower range of 66 to 50 ppm across host titanite grain 2 (Figs. 6 and A1). Overall, comparing the concentrations across the long axis of the crystal, the highest Sr values are found near the edges or 'rims' of the long axis of the host crystals, whereas the lowest Sr values are from the interior or 'cores'. Zirconium shows the opposite pattern, with higher concentrations in the interior.

5. Discussion

In the following sections, we discuss how the titanite aggregates formed, their importance in understanding the tectonic history of the Salta shear zone, and general implications these data provide in understanding the relationship between deformation and element mobility in titanite grains.

5.1. The relationship of titanite deformation with composition and age

During deformation, dislocations accumulate within grains. To reduce this build up in strain energy, dislocations may migrate to form subgrain boundaries and/or grain boundaries may migrate to form nuclei of grains with lower dislocation densities and lower strain energy (e.g. Urai et al., 1986). If terranes have been polydeformed and/or remained at high temperature conditions, the minerals may undergo multiple stages of deformation and dynamic and/or static recrystallization (e.g. Halfpenny et al., 2012). In some cases, it may be difficult to tie the microstructure to a specific event due to inheritance of intragrain low-angle boundaries (e.g. Bestmann et al., 2005) and/or due to mimicry of phases via topotactic or epitaxial growth (e.g. McNamara et al., 2012). Titanite grains are common within the WGR orthogneiss (e.g. Tucker et al., 1987; Kylander-Clark et al., 2008; Spencer et al., 2013; Garber et al., 2017). The results from previous studies show that some of the titanite grains have undergone a long-lived metamorphic history. This study highlights how some titanites have also undergone multi-stage deformation and associated recrystallization. Below we discuss the metamorphic reaction that formed the titanite followed by processes that subsequently affected the titanite grains.

In the deformed orthogneiss of the Salta shear zone, titanite grains are associated with clinozoisite and rutile. This suggests the reaction:

$$2\text{clinozoisite} + \text{rutile} + \text{quartz} = \text{titanite} + \text{anorthite} + 2H_2O$$

which is encountered during decompression (Frost et al., 2000; Kapp et al., 2009; Marsh and Kelly, 2017). The titanite grains in this sample are not simple single crystals, but rather aggregates localized within specific spatial regions of the host orthogneiss. These aggregates have a broad overall diamond or sigmoidal shape that is reminiscent of the typical morphology of metamorphic titanite grains (e.g. Kohn, 2017; Marsh and Kelly, 2017). EBSD data show that most grains within an aggregate have well-defined, straight grain boundaries (Fig. 2). The aggregate grains do not record any or minimal detectable internal misorientation variations but have large misorientation between adjacent grains (generally $>20°$). Furthermore, the titanite grains within each aggregate are not randomly oriented, but rather define a specific region in orientation space that progressively changes across the different aggregates (Fig. 3). Elements such as Sr and Zr also have broad core-to-rim zoning across the long-axis of the aggregate of grains (Figs. 6 and A1). Some of the grains do have fractures that are clear in the EBSD band contrast maps (Fig. 2); however, these fractures do not show any significant misorientation. This, combined with the well-defined, in many cases triple-junction nature of the grain boundaries, suggest the grains formed under ductile conditions rather than due to late, low-temperature brittle deformation.

The aggregate titanite grains may represent either porphyroblasts associated with metamorphism and fluids; topotactic or epitaxial growth of neoblastic titanite after older titanite and/or rutile grains; and/or recrystallization of single titanite crystals affected by later tectonic processes. Growth of neoblastic titanite by topotaxy or epitaxy on older titanite and/or rutile would result in the neoblastic titanite inheriting a preferred orientation during growth (e.g. McNamara et al., 2012). However, metamorphic or topotactic growth of titanite does not explain the systematic variation in grain orientation observed across the two aggregates unless the host phase that is being replaced had previously been deformed and recrystallized (Fig. 3). Instead, the microstructural orientations, straight grain boundaries, lack of intragrain low-angle

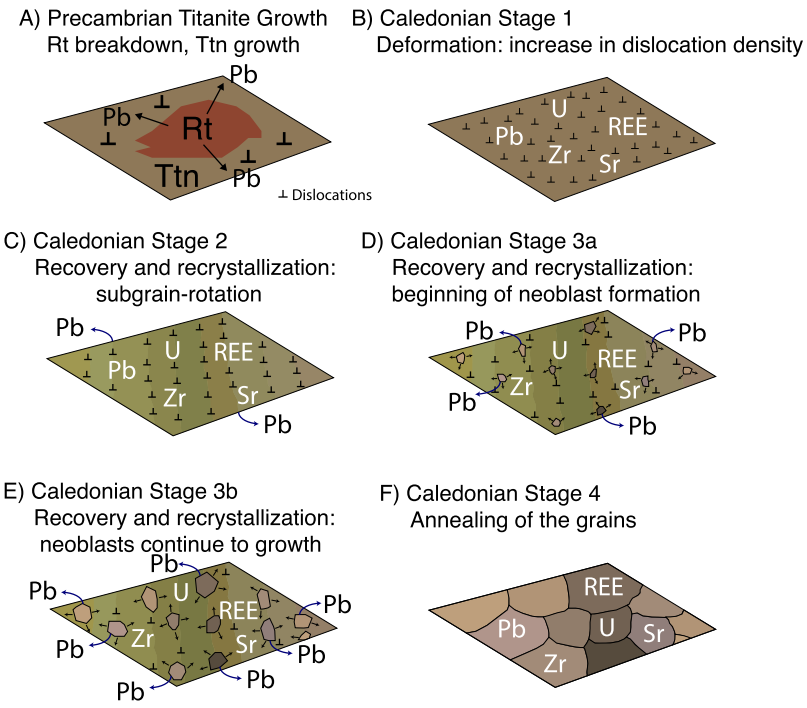

Fig. 8. Schematic representation of Salta shear zone titanite evolution. (a) Precambrian titanite growth due to the breakdown of clinozoisite and rutile; some titanite inherits radiogenic Pb from U-bearing rutile. (b) Caledonian titanite underwent plastic deformation via dislocation creep. (c) Recovery and recrystallization by subgrain-rotation causes low-angle boundaries to form across the crystal. Minor Pb loss may have occurred during subgrain-rotation. (d) Minor neoblast titanite formation during the initial stages of grain boundary migration promotes variable Pb loss, while U, Zr, Sr, and the REE remain unaffected; neoblasts are internally undeformed. (e) Neoblasts continue to grow, with continued affects on the U-Pb system. (f) Annealing of the grains results in relatively straight grain boundaries.

boundaries, chemical zoning, and high misorientation between adjacent grains are consistent with the diamond-shaped aggregates of titanite representing host, single titanite crystals that formed from the breakdown of rutile and that were subsequently affected by later tectonic processes creating the aggregate of smaller grains that are observed in the sample.

The aggregate of titanite in the highly strained gneisses of the Salta shear zone reflect a multi-stage deformation and recrystallization process (Fig. 8). Minor low-angle boundaries and the progressive change in orientation, broadly around the {010} pole in grain 1 and in the <001> axes for grain 2 (Fig. 3), indicate the host titanite crystals plastically deformed by dislocation creep, as has been interpreted for a variety of geologic phases (Fig. 8b) (Hirth and Tullis, 1992; Reddy et al., 2006; Erickson et al., 2015). Multiple dynamic and potentially late static (during the amphibolite-facies overprint) recrystallization processes reduced the strain energy produced during dislocation creep (Fig. 8c–e) (Urai et al., 1986). Evidence for intragrain deformation features, such as core and mantle structures (Hirth and Tullis, 1992), should be found in grains formed by subgrain rotation. Furthermore, misorientation would only be slightly greater than 10° between newly formed grains (e.g. Trimby et al., 1998). Instead, the lack of intragrain microstructures and the high misorientation indicate that grain-boundary migration was the final recrystallization mechanism (Fig. 8e) (Urai et al., 1986; Hirth and Tullis, 1992; Vandermeer and Juul Jensen, 1998). Subgrain rotation is commonly associated with grain boundary migration (e.g. Lloyd et al., 1997) and thus, may have preceded grain boundary migration recrystallization of the host titanite crystals (Fig. 8c). Alternatively, deformation bands or other regions of high dislocation density could have served as points where high angle grain boundaries developed (e.g. Halfpenny et al., 2012).

Neoblasts nucleated on recovered subgrain-boundaries during grain-boundary migration (e.g. Doherty et al., 1997) (Fig. 8d). The neoblastic growth resulted in strain-free grains with high misorientation angles between them (Fig. 8e) (e.g. Piazolo et al., 2012). During recrystallization, the ∼90° orientation relationship observed in parts of the aggregate grains of host titanite 1 (Fig. 3) likely represents exchange of {100} and {001}, with constant {010}, potentially because of the similar length of the a and c axes in the titanite crystal lattice. Finally, retrograde amphibolite-facies metamorphism at temperatures of 650–800°C (e.g. Walsh and Hacker, 2004) caused annealing of the grains, resulting in the end polygonal grain shapes and relatively straight grain boundaries (Fig. 8f).

Many studies have shown that the orientation of the host crystal is completely to partially inherited during recrystallization (Bestmann et al., 2005; Erickson et al., 2015). In these aggregates, the original, plastically-deformed grain has been completely replaced and thus, it is difficult to evaluate the role of orientation inheritance within the microstructure. The observed orientation pattern across the two aggregates does indicate that if the aggregate microstructure is partly inherited, the host grain must have undergone deformation prior to the recrystallization that produced the aggregate grains.

5.2. Geochronology of Salta titanite

Titanite grains may contain abundant common Pb, experience Pb loss, inherit radiogenic Pb from preexisting phases, and/or recrystallize; therefore, interpreting the U-Pb systematics and determining the crystallization or cooling age from this mineral may be challenging, especially where ^{204}Pb cannot be measured (e.g. Romer and Rötzler, 2003; Stearns et al., 2015; Garber et al., 2017; Hartnady et al., 2019). Previous studies of WGR titanite suggest that titanite grains of three different origins may be found within orthogneiss across the UHP terrane: 1) inherited Precambrian titanite, 2) recrystallized Scandian titanite, and/or 3) neoblastic Scandian titanite grains (Tucker et al., 2004; Kylander-Clark et al., 2008; Krogh et al., 2011; Spencer et al., 2013; Garber et al., 2017). Garber et al. (2017) describe specific geochemical character-

istics that they propose can be used to define the three different types of titanite, in addition to their age and texture. Precambrian titanite has the highest LREE concentrations and is more Fe-rich and Al-poor in comparison to Scandian grains. Geochemical data from Scandian titanites, combined with trace-element biotite data, are used to argue that Scandian titanite recrystallization was facilitated by a hydrous, saline brine during Scandian metamorphism.

The results of this study show that individual grains within the titanite aggregates have scatter in their U-Pb age outside of analytical uncertainty (Fig. 6). The two studied host titanite grains reveal different isotopic patterns across the aggregate. The aggregate grains in host titanite 1 all cluster near concordia (Fig. 5), suggesting that the isotopic composition of the grains was not strongly affected by the initial Pb composition or by recent Pb loss. The isotopic data from the titanite 1 aggregate define an initial $^{207}Pb/^{206}Pb$ composition within error of that predicted by the Stacey and Kramers (1975) Pb-evolution model for an age of 402 Ma (0.92 ± 0.30 versus 0.863, respectively). This initial $^{207}Pb/^{206}Pb$ composition is similar to what has been determined from previous titanite studies in the WGR (Spencer et al., 2013; Garber et al., 2017). Aggregate grains 2, 5 and 9 that are not included in the regression all border a rutile crystal, have elevated Th/U values, reveal old 207-corrected ages, and fall to the left of a best-fit regression line. These grains may have been influenced by inherited Pb from a precursor radiogenic phase (e.g., rutile) during titanite growth and/or recrystallization (e.g., Romer and Rötzler, 2003; Marsh and Kelly, 2017). Grains 2 and 9 do have elevated Sr values in comparison to the other grains. Regardless, these three grains likely have a different common Pb composition than the other aggregate grains.

In comparison, the aggregate grains within host grain 2 show much greater spread in their $^{207}Pb/^{206}Pb$ values relative to $^{238}U/^{206}Pb$ and define an initial $^{207}Pb/^{206}Pb$ value much lower in comparison to Stacey and Kramers (1975): 0.592 ± 0.035 versus 0.860 for a 363 Ma date (Fig. 5) and lower than what has been defined from previous WGR titanite data (Spencer et al., 2013; Garber et al., 2017). The low initial $^{207}Pb/^{206}Pb$ value is best explained by incorporation of radiogenic Pb from a source outside titanite. Throughout the thin section, and evidenced in host grain 1, the titanite formed partially from the breakdown of rutile (Fig. 2). Host titanite 2 may have incorporated radiogenic Pb from rutile during rutile breakdown associated with titanite growth. Analyzed rutile is low in U (27–29 ppm), and the titanite in aggregate 2 also has very low U concentrations (19 to <1 ppm). Romer and Rötzler (2003) also describe titanite crystals from several samples that grew and experienced the same P–T history but yield a variety of ages due to radiogenic inheritance from precursor rutile and/or post-peak recrystallization of titanite enhanced by fluids and deformation. Notably, only some of the titanite show evidence for radiogenic inheritance, not all of the grains. The aggregate of grains within titanite 2 also show a spatial trend in isotopic composition. The majority of the grains comprising the left side of the aggregate have higher common to radiogenic Pb ratios in comparison to the rest of the aggregate (Fig. 5). This trend may also reflect some degree of sector zoning in the host titanite crystal that had developed prior to Scandian deformation and recrystallization.

Titanite U-Pb regression lines provide important insight into aggregates and their interpretation as either 1) a mix of radiogenic and common Pb (aggregate 1 with an initial $^{207}Pb/^{206}Pb$ composition that matches with Stacey and Kramers (1975)), versus 2) a mix of three Pb components including, regional common Pb, *in situ* radiogenic Pb, and an additional distinct inherited radiogenic component (aggregate 2 with its low $^{207}Pb/^{206}Pb$ composition). In comparison, the calculated 207-corrected ages provide additional information on what is happening on the intergrain-scale within the aggregate. The calculated 207-corrected ages and the uncorrected $^{238}U/^{206}Pb$ dates together reveal that both aggregates comprise a mixture of grains completely reset during the Caledonian and others with inherited Precambrian Pb. We interpret any titanite grain with a 207-corrected date older than ca. 409 Ma to reflect this inherited component (Fig. 6) (DesOrmeau et al., 2015). Furthermore, because some of the titanite grains within the aggregates have an inherited Precambrian isotopic composition, the rutile to titanite breakdown reaction occurred prior to terminal Scandian processes. Garber et al. (2017) note rutile and zircon inclusions within many of their studied Precambrian titanites, supporting pre-Scandian rutile-to-titanite-reactions.

5.3. The relationship between titanite deformation and trace-element mobility

Multiple studies have shown that important accessory minerals used for petrochronology, including zircon (Reddy et al., 2006; Piazolo et al., 2012, 2016), monazite (Erickson et al., 2015), and titanite (Müller and Franz, 2004; Bonamici et al., 2015), among others, can be affected by crystal-plastic deformation. For example, atom-probe studies of zircon show that dislocations act as element sinks, collecting and concentrating trace elements, such as U and other solute elements, as they move through the crystal lattice (Piazolo et al., 2016; Reddy et al., 2016). In some cases, dislocation arrays can facilitate pipe diffusion of incompatible elements, including Pb (Reddy et al., 2006; Piazolo et al., 2016).

In the WGR titanite described here, the individual aggregate grains within the host titanites reveal a mix of Scandian and inherited 207-corrected ages (Figs. 5, 6, and A3). The scatter of the age distribution across the aggregates suggests that the host titanite grains experienced variable Pb loss during recrystallization (Fig. 8). Recrystallization may have been driven by fluids and/or deformation (e.g., Lucassen and Becchio, 2003; Garber et al., 2017). We favor a model in which both deformation and fluids impacted the trace element and isotopic systems of Salta titanite grains based on observations of chemical zoning within aggregate grains, the inherited 207-corrected ages, and evidence for grain boundary migration recrystallization. We discuss these topics below as well as their implications for interpreting *P-T-t* histories using titanite.

Some fluids were likely present during Salta shear zone activity associated with retrogression and exhumation of the gneisses. The patchy zoning in Ca, Ti, and Al within the titanite (Fig. 4) was mostly likely produced by fluid alteration of the titanite grains, with fluids penetrating along the grain boundaries. The fluids may also have affected the isotopic system of the titanites (e.g., Garber et al., 2017). However, the inherited titanite dates recorded in this study are younger (<650 Ma) than that which has previously been described for WGR titanites that show evidence of Pb diffusion but still yield demonstrably Precambrian dates (ca. 1600–950 Ma) (see summary in Garber et al., 2017). The inherited grains of this study may have had a different common Pb composition, and thus, the 207-corrected ages may not be entirely accurate. Similar problems with the 207-correction, though, should have affected inherited titanite in other WGR studies that report Precambrian titanite ages. In titanite 2, the inheritance of radiogenic Pb could account for the younger inherited 207-corrected ages (ca. 440–646 Ma); however, this does not explain the young inherited ages observed in aggregate grain 1 (ca. 460–580 Ma), where there is no evidence for an inherited radiogenic composition from rutile. The main difference between the samples studied herein and those studied in previous work is that the gneiss and the titanite within this gneiss of this study were affected by high strain, whereas most of the samples that yielded Precambrian titanite dates in previous work did not show evidence of Scandian deformation.

Given the clear evidence for deformation and associated recrystallization affecting titanite grain orientations within the aggre-

gates (Fig. 3), these factors must have also affected their isotopic composition during aggregate formation from the original titanite grains. Some Pb loss may have occurred during subgrain-rotation recrystallization and the formation of dislocation walls (Fig. 8c). Following subgrain rotation, a switch to recrystallization by a grain boundary migration process gave rise to neoblastic titanite to form the observed grain aggregates. The mobility of grain boundaries during neoblastic grain growth has been shown to be an effective mechanism of removing Pb from other accessory phases, for example monazite (Erickson et al., 2015). This reflects the higher diffusivity of grain boundaries relative to low-angle boundaries and dislocations and the more effective recrystallization mechanism for moving the grain boundary through the plastically deformed subgrained titanite. Thus, radiogenic Pb was not incorporated or was only partially incorporated into the neoblastic grains during the grain-boundary migration resulting in the variability in dates across the grain aggregates (cf. Erickson et al., 2015). We interpret that grain-boundary migration was the main recrystallization mechanism that affected the U-Pb system in the shear zone titanite. The sub-grain rotation and grain-boundary migration recrystallization associated with strain minimization likely occurred as stress was diminishing and thus dislocation creep was slowing or ceased to occur and instead, diffusional processes dominated within the grains (e.g., Frost and Ashby, 1982). Thus, the grain-boundary migration and associated Pb-loss most likely occurred at the end of deformation within the shear zone after the UHP rocks had been exhumed to mid-crustal depths and underwent amphibolite-facies metamorphism (Renedo et al., 2015).

As noted above, fluids were likely also present in the shear zone, especially during amphibolite-facies metamorphism. Given the patchy zoning within the individual grain aggregates, the fluids were present either syn-recrystallization during grain-boundary migration or post-recrystallization. If present during deformation and shear zone activity, the fluids would only have increased grain-boundary mobility and accelerated the rate of recrystallization processes affecting the titanite (e.g. Urai et al., 1986; Gottstein and Shvindlerman, 2010). Thus, the combination of deformation and fluids resulted in the younger inherited ages observed in this study compared to previous WGR titanite studies.

Previous studies have argued that both U-Pb and trace element systems in titanite grains are equally affected by recrystallization (e.g. Storey et al., 2007; Stearns et al., 2015). Garber et al. (2017) concluded that there was no evidence for Precambrian Zr inheritance in the recrystallized WGR Caledonian titanite grains but did find Zr and other trace element inheritance (except for Pb) in the core of titanites that yielded partially reset U-Pb dates. This decoupling between the Pb and other trace-elements is found in undeformed titanite or in titanite with some deformation twinning. In the Salta titanite, the REE, Sr, and Zr do not show a correlation with the U-Pb age or to the major element abundances (e.g., Ca, Ti, and Al), nor do they show any correlation with proximity to the rutile in the grain aggregate of titanite 1 (Figs. 6, 7, S1). The distribution of Sr and Zr contents across the long axis of the aggregate grains, with higher Zr and lower Sr concentrations in the host grain centers, is consistent with growth or alteration of single euhedral titanite that would have crystallized during the Precambrian as part of the granulite-facies event that affected the protolith to the WGR rocks (e.g. Tucker et al., 2004). The Zr, Sr, and REE patterns across the grains do not appear to have been affected by the multi-stage recrystallization of the host euhedral titanite grains or by the fluids that affected the individual aggregate grains. Thus, our results, combined with other recent work (e.g. Kirkland et al., 2016), document that the U-Pb isotopic system was affected in a different manner than other key trace elements that have been used to link titanite ages with the P–T path during deformation and associated recrystallization and fluid flow. This is despite the similar ionic radii and substitution site between, for example, Pb and Sr. In titanite from this highly deformed WGR gneiss, trace elements are decoupled from the U-Pb system (Fig. 6).

6. Conclusions

The robust interpretation of geochemical and geochronological data from titanite requires an understanding of how trace element mobility is affected by metamorphism and deformation in high-grade terranes. All the microstructural and compositional characteristics observed in the shear zone titanite crystals from the WGR are consistent with crystal-plastic deformation of a Precambrian titanite grain followed by grain boundary migration recrystallization and the formation of an aggregate of strain-free crystals during Caledonian orogenesis (Fig. 8).

This study documents the dissimilar influence of deformation and fluids on both U-Pb isotopes and trace-element composition in dynamically and statically recrystallized titanite crystals. The U-Pb isotopes and trace elements are decoupled as a result of a multi-stage recrystallization process coupled with fluid mobility in a shear zone in the Western Gneiss Region, Norway. A comparison of U-Pb data and trace element distribution suggests this decoupling; however, EBSD analyses are powerful in deciphering the deformation and associated recrystallization history that affected the isotopic system of titanite and other accessory phases. This result highlights the importance of integrating microstructural and compositional mapping for titanite U-Pb geochronology and Zr-in-titanite thermobarometry in order to relate pressure, temperature, and time in deformed rocks.

CRediT authorship contribution statement

There are 8 authors on this manuscript. C. Kirkland completed the modeling and calculation of the 207-corrected ages and f207%. S. Reddy assisted in collecting and producing figures of the EBSD data. H. Blatchford, D. Whitney, and C. Teyssier have worked with S. Gordon for multiple years in the Western Gneiss Region. Blatchford sent Gordon the thin sections for analyses and helped to develop Fig. S1. Whitney and Teyssier assisted in the selection of the sample and interpretation of the data. N. Evans and B. McDonald are the laboratory managers for the LA-ICP-MS. They assisted in setting up the LA-ICP-MS analyses. Gordon developed the overall project, collected all of the data (with the assistance of those listed above), and wrote the first draft of the manuscript. All of the co-authors have edited the manuscript and approved it for submission.

Declaration of competing interest

The authors declare that they have no known competing financial interests or personal relationships that could have appeared to influence the work reported in this paper.

Acknowledgements

We thank Malcolm Roberts for his assistance with the EPMA analyses. This manuscript greatly benefited from comments by Chloe Bonamici, Josh Garber, Zachary Michels, Mark Pearce, Frank Spear, and Mike Stearns. We also acknowledge the facilities, and the scientific and technical assistance of the Australian Microscopy & Microanalysis Research Facility at the Centre for Microscopy, Characterisation & Analysis, the University of Western Australia, a facility funded by the University, State and Commonwealth Governments. Analysis in the GeoHistory Facility, JdLC was enabled by AuScope (http://auscope.org.au) and the Australian Government via the National Collaborative Research Infrastructure Strategy (NCRIS).

Funding

This work was supported by the National Science Foundation (grants EAR-1624546, EAR-1827198 and EAR-1062187 to Gordon, EAR-1040980 to Whitney, and EAR-1827220 to Teyssier) and the Australian Research Council (grant DP160104637 and LE130100053 to Reddy).

Appendix A. Supplementary material

Supplementary material related to this article can be found online at https://doi.org/10.1016/j.epsl.2021.116810.

References

Bestmann, M., Piazolo, S., Spiers, C.J., Prior, D.J., 2005. Microstructural evolution during initial stages of static recovery and recrystallization: new insights from in-situ heating experiments combined with electron backscatter diffraction analysis. J. Struct. Geol. 27, 447–457. https://doi.org/10.1016/j.jsg.2004.10.006.

Bonamici, C.E., Fanning, C.M., Kozdon, R., Fournelle, J.H., Valley, J.W., 2015. Combined oxygen-isotope and U-Pb zoning studies of titanite: new criteria for age preservation. Chem. Geol. 398, 70–84. https://doi.org/10.1016/j.chemgeo.2015.02.002.

Carswell, D.A., Brueckner, H.K., Cuthbert, S.J., Mehta, K., O'Brien, P.J., 2003. The timing of stabilization and the exhumation rate for ultra-high pressure rocks in the Western Gneiss Region of Norway. J. Metamorph. Geol. 21, 601–612.

Cherniak, D.J., 1993. Lead diffusion in titanite and preliminary results on the effects of radiation damage on Pb transport. Chem. Geol. 110, 177–194.

Cuthbert, S.J., Carswell, D.A., Krogh-Ravna, E.J., Wain, A., 2000. Eclogites and eclogites in the Western Gneiss region, Norwegian Caledonides. Lithos 52, 165–195.

DesOrmeau, J.W., Gordon, S.M., Kylander-Clark, A.R.C., Hacker, B.R., Bowring, S.A., Schoene, B., Samperton, K.M., 2015. Insights into (U)HP metamorphism of the Western Gneiss Region, Norway: a high-spatial resolution and high-precision zircon study. Chem. Geol. 414, 138–155. https://doi.org/10.1016/j.chemgeo.2015.08.004.

Doherty, R.D., Hughes, D.A., Humphreys, F.J., Jonas, J.J., Juul Jensen, D., Kassner, M.E., King, W.E., McNelley, T.R., McQueen, H.J., Rollett, A.D., 1997. Current issues in recrystallization: a review. Mater. Sci. Eng. A 238, 219–274.

Engi, M., 2017. Petrochronology based on REE-minerals: monazite, allanite, xenotime, apatite. In: Kohn, M.J., Engi, M., Lanari, P. (Eds.), Petrochronology: Methods and Applications. In: Reviews in Mineralogy and Geochemistry, vol. 83, pp. 365–418.

Erickson, T.M., Pearce, M.A., Taylor, R.J.M., Timms, N.E., Clark, C., Reddy, S.M., Buick, I.S., 2015. Deformed monazite yields high-temperature tectonics ages. Geology 43, 383–386. https://doi.org/10.1130/G36533.1.

Frost, H.J., Ashby, M.F., 1982. Deformation-Mechanism Maps, the Plasticity and Creep of Metals and Ceramics. Pergamon Press, Oxford.

Frost, B.R., Chamberlain, K.R., Schumacher, J.C., 2000. Sphene (titanite): phase relations and role as a geochronometer. Chem. Geol. 172, 131–148.

Garber, J.M., Hacker, B.R., Kylander-Clark, A.R.C., Stearns, M., Seward, G., 2017. Controls on trace element uptake in metamorphic titanite: implications for petrochronology. J. Petrol. 58, 1031–1057. https://doi.org/10.1093/petrology/egx046.

Gordon, S.M., Whitney, D.L., Teyssier, C., Fossen, H., 2013. U-Pb dates and trace-element geochemistry of zircon from migmatite, Western Gneiss Region, Norway: significance for history of partial melting in continental subduction. Lithos 170–171, 35–53.

Gottstein, G., Shvindlerman, L.S., 2010. Grain Boundary Migration in Metals: Thermodynamics, Kinetics, Applications. CRC Press, Boca Raton, Florida.

Hacker, B.R., 2006. Pressures and temperatures of ultrahigh-pressure metamorphism: Implications for UHP tectonics and H_2O in subducting slabs. Int. Geol. Rev. 48, 1053–1066.

Hacker, B.R., Kylander-Clark, A.R.C., Holder, R., Andersen, T.B., Peterman, E.M., Walsh, E.O., Munnikhuis, J.K., 2015. Monazite response to ultrahigh-pressure subduction from U-Pb dating by laser ablation split stream. Chem. Geol. 409, 28–41. https://doi.org/10.1016/j.chemgeo.2015.05.008.

Halfpenny, A., Prior, D.J., Wheeler, J., 2012. Electron backscatter diffraction analysis to determine the mechanisms that operated during dynamic recrystallization of quartz-rich rocks. J. Struct. Geol. 36, 2–15. https://doi.org/10.1016/j.jsg.2012.01.001.

Hartnady, M.I.H., Kirkland, C.L., Clark, C., Spaggiari, C.V., Smithies, R.H., Evans, N.J., McDonald, B.J., 2019. Titanite dates crystallization: slow Pb diffusion during super-solidus re-equilibration. J. Metamorph. Geol. 37, 823–838. https://doi.org/10.1111/jmg.12489.

Hayden, L.A., Watson, E.B., Wark, D.A., 2008. A thermobarometer for sphene (titanite). Contrib. Mineral. Petrol. 155, 529–540.

Holder, R.M., Hacker, B.R., Seward, G.G.E., Kylander-Clark, A.R.C., 2019. Interpreting titanite U-Pb dates and Zr thermobarometry in high-grade rocks: empirical constraints on elemental diffusivities of Pb, Al, Fe, Zr, Nb, and Ce. Contrib. Mineral. Petrol. 174. https://doi.org/10.1007/s00410-019-1578-2.

Hirth, G., Tullis, J., 1992. Dislocation creep regimes in quartz aggregates. J. Struct. Geol. 14, 145–159.

Kapp, P., Manning, C.E., Tropper, P., 2009. Phase-equilibrium constraints on titanite and rutile activities in mafic epidote amphibolites and geobarometry using titanite-rutile equilibria. J. Metamorph. Geol. 27, 509–521. https://doi.org/10.1111/j.1525-1314.2009.00836.x.

Kirkland, C.L., Spaggiari, C.V., Johnson, T.E., Smithies, R.H., Danisík, M., Evans, N., Wingate, M.T.D., Clark, C., Spencer, C., Mikucki, E., McDonald, B.J., 2016. Grain size matters: implications for element and isotopic mobility in titanite. Precambrian Res. 278, 283–302. https://doi.org/10.1016/j.precamres.2016.03.002.

Kohn, M.J., 2017. Titanite petrochronology. Rev. Mineral. Geochem. 83, 419–441. https://doi.org/10.2138/rmg.2017.83.13.

Krabbendam, M., Dewey, J.F., 1998. Exhumation of UHP rocks by transtension in the Western Gneiss Region, Scandinavian Caledonides. In: Holdsworth, R.E.S., Dewey, J.F. (Eds.), Continental Transpressional and Transtensional Tectonics. Geological Society Special Publications, London, pp. 159–181.

Krabbendam, M., Wain, A., Andersen, T.B., 2000. Pre-Caledonian granulite and gabbro enclaves in the Western Gneiss Region, Norway: indications of incomplete transition at high pressure. Geol. Mag. 137, 235–255. https://doi.org/10.1017/S0016756800004015.

Krogh, T.E., Kamo, S.L., Robinson, P., Terry, M.P., Kwok, K., 2011. U-Pb zircon geochronology of eclogites from the Scandian orogen, northern Western Gneiss Region, Norway: 14-20 Myr between eclogite crystallization and return to amphibolite-facies conditions. Can. J. Earth Sci. 48, 441–472.

Kylander-Clark, A.R.C., Hacker, B.R., 2014. Age and significance of felsic dikes from the UHP Western Gneiss Region. Tectonics 33. https://doi.org/10.1002/2014TC003582.

Kylander-Clark, A.R.C., Hacker, B.R., Mattinson, J.M., 2008. Slow exhumation of UHP terranes: titanite and rutile ages of the Western Gneiss Region, Norway. Earth Planet. Sci. Lett. 272, 531–540.

Lloyd, G.E., Farmer, A.B., Mainprice, D., 1997. Misorientation analysis and the formation and orientation of subgrain and grain boundaries. Tectonphysics 279, 55–78.

Lucassen, F., Becchio, R., 2003. Timing of high-grade metamorphism: Early Palaeozoic U-Pb formation ages of titanite indicate long-standing high-T conditions at the western margin of Gondwana (Argentina, 26–29°S). J. Metamorph. Geol. 21, 649–662.

Lucassen, F., Dulski, P., Abart, R., Franz, G., Rhede, D., Romer, R.L., 2010. Redistribution of HFSE elements during rutile replacement by titanite. Contrib. Mineral. Petrol. 160, 279–295. https://doi.org/10.1007/s00410-009-0477-3.

Lucassen, F., Franz, G., Dulski, P., Romer, R.L., Rhede, D., 2011. Element and Sr isotope signatures of titanite as indicator of variable fluid composition in hydrated eclogite. Lithos 121, 12–24. https://doi.org/10.1016/j.lithos.2010.09.018.

Marsh, J.H., Kelly, E.D., 2017. Petrogenetic relations among titanium-rich minerals in an anatectic high-P mafic granulite. J. Metamorph. Geol. 35, 717–738. https://doi.org/10.1111/jmg.12252.

McNamara, D.D., Wheeler, J., Pearce, M., Prior, D.J., 2012. Fabrics produced mimetically during static metamorphism in retrogressed eclogites from the Zermatt-Saas zone, Western Italian Alps. J. Struct. Geol. 44, 167–178. https://doi.org/10.1016/j.jsg.2012.08.006.

Mezger, K., Rawnsley, C., Bohlen, S., Hanson, G., 1991. U-Pb garnet, sphene, monazite, and rutile ages: implications for the duration of high grade metamorphism and cooling histories, Adirondack Mts., New York. J. Geol. 99, 415–428.

Milnes, A.G., Koyi, H.A., 2000. Ductile rebound of an orogenic root: case study and numerical model of gravity tectonics in the Western Gneiss Complex, Caledonides, southern Norway. Terra Nova 12, 1–7.

Müller, W.F., Franz, G., 2004. Unusual deformation microstructures in garnet, titanite, and clinozoisite from an eclogite of the Lower Schist Cover, Tauern Window, Austria. Eur. J. Mineral. 16, 939–944. https://doi.org/10.1127/0935-1221/2004/0016-0939.

Paton, C., Hellstrom, J., Paul, B., Woodhead, J., Hergt, J., 2011. Iolite: freeware for the visualization and processing of mass spectrometric data. J. Anal. At. Spectrom. 26, 2508–2518.

Piazolo, S., Austrheim, H., Whitehouse, M., 2012. Brittle-ductile microfabrics in naturally deformed zircon: deformation mechanisms and consequences for U-Pb dating. Am. Mineral. 97, 1544–1563. https://doi.org/10.2138/am.2012.3966.

Piazolo, S., La Fontaine, A., Trimby, P., Harley, S., Yang, L., Armstrong, R., Cairney, J.M., 2016. Deformation-induced trace element redistribution in zircon revealed using atom probe tomography. Nat. Commun. 7, 10490. https://doi.org/10.1038/ncomms10490.

Ravna, E.J., Terry, M.P., 2004. Geothermobarometry of UHP and HP eclogites and schists - an evaluation of equilibria among garnet-clinopyroxene-kyanite-phengite-coesite/quartz. J. Metamorph. Geol. 22, 579–592. https://doi.org/10.1111/j.1525-1314.2004.00534.x.

Reddy, S.M., Timms, N.E., Trimby, P., Kinny, P.D., Buchan, C., Blake, K., 2006. Crystal-plastic deformation of zircon: a defect in the assumption of chemical robustness. Geology 34, 257–260.

Renedo, R.N., Nachlas, W.O., Whitney, D.L., Teyssier, C., Piazolo, S., Gordon, S.M., Fossen, H., 2015. Fabric development during exhumation from ultrahigh-pressure in an eclogite-bearing shear zone, Western Gneiss Region, Norway. J. Struct. Geol. 71, 58–70. https://doi.org/10.1016/j.jsg.2014.09.012.

Roberts, D., Gee, D.G., 1985. An introduction to the structure of the Scandinavian Caledonides. In: Gee, D.G., Sturt, B.A. (Eds.), The Caledonide Orogen—Scandinavia and Related Areas. Wiley, Chichester, UK, pp. 55–68.

Romer, R.L., Rötzler, J., 2003. Effect of metamorphic reaction history on the U-Pb dating of titanite. In: Vance, D., Müller, W., Villa, I.M. (Eds.), Geochronology: Linking the Isotopic Record with Petrology and Textures, vol. 220. Geological Society of London, pp. 147–158.

Root, D.B., Hacker, B.R., Mattinson, J.M., Wooden, J.L., 2005. Zircon geochronology and ca. 400 Ma exhumation of Norwegian ultrahigh-pressure rocks: an ion microprobe and chemical abrasion study. Earth Planet. Sci. Lett. 228, 325–341.

Rubatto, D., 2002. Zircon trace element geochemistry: partitioning with garnet and the link between U-Pb ages and metamorphism. Chem. Geol. 184, 123–138.

Spencer, K.J., Hacker, B.R., Kylander-Clark, A.R.C., Andersen, T.B., Cottle, J.M., Stearns, M.A., Poletti, J.E., Seward, G.G.E., 2013. Campaign-style titanite U-Pb dating by laser-ablation ICP: implications for crustal flow, phase transformations and titanite closure. Chem. Geol. 341, 84–101.

Stacey, J.S., Kramers, J.D., 1975. Approximation of terrestrial lead isotope evolution by a two-stage model. Earth Planet. Sci. Lett. 26, 207–221.

Stearns, M.A., Hacker, B.R., Ratschbacher, L., Rutte, D., Kylander-Clark, A.R.C., 2015. Titanite petrochronology of the Pamir gneiss domes: implications for middle to deep crust exhumation and titanite closure to Pb and Zr diffusion. Tectonics 34, 784–802. https://doi.org/10.1002/2014TC003774.

Storey, C.D., Smith, M.P., Jeffries, T.E., 2007. In situ LA-ICP-MS U-Pb dating of metavolcanics of Norrbotten, Sweden: records of extended geological histories in complex titanite grains. Chem. Geol. 240, 163–181.

Trimby, P.W., Prior, D.J., Wheeler, J., 1998. Grain boundary hierarchy development in a quartz mylonite. J. Struct. Geol. 20, 913–935.

Tucker, R.D., Råheim, A., Krogh, T.E., Corfu, F., 1987. Uranium-lead zircon and titanite ages from the northern portion of the Western Gneiss Region, south-central Norway. Earth Planet. Sci. Lett. 81, 203–211.

Tucker, R.D., Krogh, T.E., Råheim, A., 1990. Proterozoic evolution and age-province boundaries in the central part of the Western Gneiss Region, Norway: results of U-Pb dating of accessory minerals from Trondheimsfjord to Geiranger. In: Gower, C.F., Rivers, T., Ryan, B. (Eds.), Mid-Proterozoic Laurentia–Baltica, Special Paper, Vol. 38. Geological Association of Canada, pp. 149–173.

Tucker, R.D., Robinson, P., Solli, A., Gee, D.G., Thorsnes, T., Krogh, T.E., Nordgulen, Ø., Bickford, M.E., 2004. Thrusting and extension in the Scandian hinterland, Norway: new U–Pb ages and tectonostratigraphic evidence. Am. J. Sci. 304 (6), 477–532. https://doi.org/10.2475/ajs.304.6.477.

Urai, J.L., Means, W.D., Lister, G.S., 1986. Dynamic recrystallization of minerals. Geophys. Monogr. 36, 161–200.

Vandermeer, R.A., Juul Jensen, D., 1998. The migration of high angle grain boundaries during recrystallization. Interface Sci. 6, 95–104.

Wain, A., 1997. New evidence for coesite in eclogite and gneisses: defining an ultrahigh-pressure province in the Western Gneiss region of Norway. Geology 25, 927–930.

Wain, A.L., Waters, D.J., Austrheim, H., 2001. Metastability of granulites and processes of eclogitisation in the UHP region of western Norway. J. Metamorph. Geol. 19, 609–625.

Walsh, E.O., Hacker, B.R., 2004. The fate of subducted continental margins: two-stage exhumation of the high-pressure to ultrahigh-pressure Western Gneiss Region, Norway. J. Metamorph. Geol. 22, 671–687. https://doi.org/10.1111/j.1525-1314.2004.00541.x.